PAPER

iGrab: hand orthosis powered by twisted and coiled polymer muscles

IOP Publishing Smart Materials and Structures
Smart Mater. Struct. 26 (2017) 105048 (14pp) https://doi.org/10.1088/1361-665X/aa8929

iGrab: hand orthosis powered by twisted and coiled polymer muscles

Lokesh Saharan[1,4], Monica Jung de Andrade[2], Wahaj Saleem[3], Ray H Baughman[2] and Yonas Tadesse[1,2]

[1] Humanoid, Bio-robotics and Smart Systems (HBS) Laboratory, Mechanical Engineering Department, The University of Texas at Dallas, Richardson, TX 75080, United States of America
[2] Alan G. MacDiarmid NanoTech Institute, The University of Texas at Dallas, Richardson, TX 75080, United States of America
[3] Lynntech Inc., 2501 Earl Rudder Fwy #100, College Station, TX 77845, United States of America

E-mail: lokeshbsaharan@gmail.com and yonas.tadesse@utdallas.edu

Received 8 May 2017, revised 2 August 2017
Accepted for publication 30 August 2017
Published 22 September 2017

Abstract

Several works have been reported in powered hand orthosis in the last ten years for assistive or rehabilitative purposes. However, most of these approaches uses conventional actuators such as servo motors to power orthosis. In this work, we demonstrate the recently reported twisted and coiled polymeric (TCP) muscles to drive a compact, light, inexpensive and wearable upper extremity device, iGrab. A 3D printed orthotic hand module was designed, developed and tested for the performance. The device has six 2-ply muscles of diameter 1.35 mm with a length of 380 mm. We used a single 2-ply muscle for each finger and two 2-ply muscles for the thumb. Pulsed actuation of the muscles at 1.8 A current for 25 s with 7% duty cycle under natural cooling showed full flexion of the fingers within 2 s. Modeling and simulation were performed on the device using standard Euler–Lagrangian equations. Our artificial muscles powered hand orthosis demonstrated the capability of pinching and picking objects of different shapes, weights, and sizes.

Keywords: powered orthosis, artificial muscles, design, hand exoskeleton, upper limb extremity, orthotic hand

(Some figures may appear in colour only in the online journal)

1. Introduction

The quality of life may be severely affected by the partial or complete loss of hand function as a result of muscle or nerve disorders. For instance, there are as many as 4.1 million Americans who suffer from impairment of the upper extremity [1], muscular disorders such as multiple sclerosis, Parkinson's disease or loss of upper limb function due to stroke. This work addresses the need for these patients via the design, development, and testing of a hand orthosis (figure 1) based on novel twisted and coiled polymer (TCP) actuators, 3D printed ring structures, tendons, tendon routing channels, pulleys and rubber strips.

Extensive works [2, 3] have revealed the working principles of natural muscles for performing flexion, extension, abduction and adduction. Including studies show the use of flex sensors [4] for the control of the orthotic devices along with ionic polymer metal composites for biomimetic applications [5–7]. Additionally, kinematic and dynamic models [8–10] were used for evaluation of the mechanics of natural hand and fingers.

Orthotic devices can be mainly classified as passive or active. Even though most of the studies previously focused on passive orthoses (also known as splints) [11–15] in the last few years, more efforts were made in the design and development of active orthoses. It was demonstrated that active devices not only have the assistive role, but also decrease the rehabilitation period. Orthotic hand devices presented in the literature have addressed various aspects and requirements in a non-comprehensive way. Some of them considered the degrees of freedom as a prime concern while others emphasized overall weight; still, others found control strategies as the primary factor.

Material selection is imperative as ergonomics, cost and efficiency of the device depend on it. Macovei and Doroftei

[4] Author to whom any correspondence should be addressed.

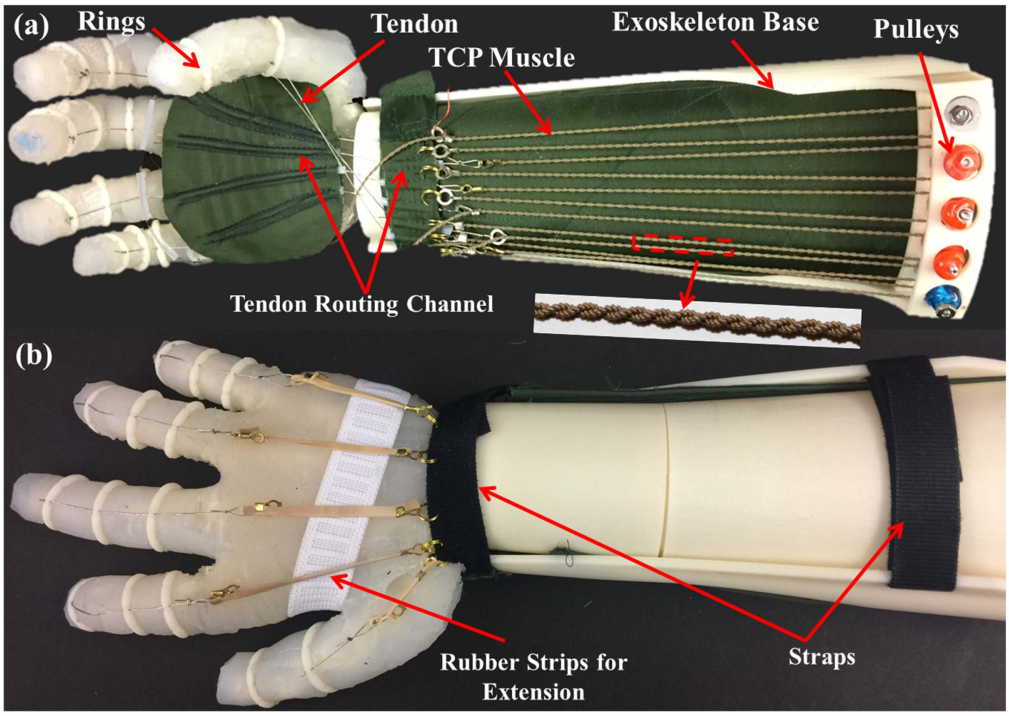

Figure 1. iGrab orthotic hand (a) Front side of the fully assembled exoskeleton mounted on the test bad hand, and (b) the back side of the exoskeleton showing extension mechanism and straps.

[16] have summarized upper limb rehabilitation devices. The first exoskeletons were made of metal, bulky, and inconvenient to wear for lengthy periods [17–20]. Later, ergonomic models that combined metal and polymeric parts were presented. Recently, lighter orthotic hands made of polymers [21–26] or soft fabrics and other materials [27–29] were reported. Regarding actuation technologies, most of the orthotic hands in the literature utilized conventional actuators such as DC motors [17, 21, 23, 27, 30, 31], which are bulky and difficult to incorporate into designs where space is constrained. Some researchers have tried pneumatic actuators [22, 26], which are bulky and inconvenient due to the need for a source of compressed air. A myoelectric hand [32] is among the few, which uses smart actuators such as shape memory alloys (SMA). SMAs can generate high stress, but the significant drawback is the large hysteresis loop typically observed in the stress-strain curves and high cost [33–35] followed by low efficiency due to Joule heating. Also, the stroke of the SMA wire is around 4%–5% which is very less. During this study, we have calculated that a minimum of 50 mm of the tendon displacement (discussed in later section) is required to fully actuate a human finger. Then, with the 5% actuation, we would require around 1 m long SMA to actuate the finger. Such a large length of actuator would require high power to actuate causing a high amount of heat loss apart from being expensive (around $3000/kg).

Twisted and coiled polymer (TCP) muscles [35] were recently discovered by Haines *et al* as a new class of smart actuators having high power to weight ratio. These materials can be fabricated using commercially available sewing thread by twist insertion under a particular load. These twisted and coiled muscles need to be annealed and trained before using as actuators. These muscles have a high linear stroke as high as 49% [35] and have other advantages over conventional actuators such as lightweight, low-cost of material ($5/kg for the raw material) and easily fabricated. These muscles have been studied for their characterization and applications [36–41]. In our recent works, we have shown the various application of this new actuator for robotic finger [42], tensegrity structure [43], the musculoskeletal system [44] and artificial skin for facial expressions [45]. The only issue with these materials is its efficiency which is close to 1%. To resolve these matters, we have presented locking mechanism for robotic systems in our recent work [46]. The locking mechanism was designed and developed during the study and incorporated in a prosthetic hand that can be adapted to orthotic hand. The locking mechanism utilized three linear TCP actuators to allow retaining a particular position during the fixed gestures and holding of the objects for longer duration. One of them is actuated to open up a spring loaded conical structure where tendons are connected with the other muscles for flexion and extension. Results showed that the mechanism can hold around 3.5 N of force with around 4.5% of slippage. The details are found in Saharan and Tadesse [46].

The TCP muscles are slow when actuated with regular actuation (heating with square wave input voltage), because the time required to cool under natural conditions at the room temperature. However, pulsed actuation (high intensity heating with electrical pulse) enables the device to actuate faster 1 Hz or higher frequency. In our previous study [35], we have shown 1 Hz, 5 Hz and 7.5 Hz frequency level for these muscles can be achieved using active cooling. The control system component and implementation is out of scope for this study, but in future we will present the high frequency control

Table 1. Precursor material and TCP muscles (2-ply) characteristics.

Properties	Precursor yarn multifilament	2-ply TCP
Number of filaments	n = 136	272 (2n)
Diameter, d (mm)	0.20	0.85
Linear density (mg/cm)	1.3	8.3 (±0.5)
Optimum load for actuation (g)	—	300
Operating temperature (°C)	25–225	25–225
Actuation (%)	0–4	0–16

of the system. The current focus of this paper is on the mechanical design, device performance, integration and characterization.

This paper demonstrates the design, prototype fabrication, modeling and characterization of a new hand orthosis called 'iGrab' [47] powered by nylon based TCP muscles (figure 1). Experiments were conducted by mounting the iGrab device on a custom-made biomimetic dummy hand focusing on the full hand flexion and extension with emphasis on the thumb. The iGrab device provides the full flexion and extension movements of all the digits. Tests on the device showed a capability of pinching movements for manipulating objects of different shapes and sizes. The next section elaborates the motivation behind the work and the actuator. Then, we will discuss the design of our orthotic hand, followed by experimental studies on the prototype. Finally, modeling, validation, and manipulation capabilities of the device will be presented.

2. Design requirements of orthotic device

2.1. Motivation

Most of the devices reported in the literature are bulky and ergonomically not suitable to use as an everyday companion for patients. The reasons can be different aspects. The hand orthosis should be lightweight and customizable to individual needs since disabilities varies to each person. That is where 3D printing proves to be a boon as one can quickly modify designs to make a fit for individual and then manufacture it rapidly. Apart from 3D printing, TCP muscles are light in weight, easy to fabricate and make the device easily customizable. So, 3D printed exoskeleton can be easily converted to a wearable glove by assembling them in a thermally regulated polymer that prevents heat to the users since the polymer muscles are thermally actuated.

2.2. TCP artificial muscles for orthosis

The artificial muscles for our orthotic hand are made of twisted and coiled polymer thread. The thread is commercially available precursor fiber; conductive multifilament silver coated nylon 6,6 sewing thread manufactured by Shieldex Trading, Inc. (Shieldex PN#260151023534). The specification of this thread is given in table 1, and it was selected for the present study. We have used two ply muscle for the flexion and rubber bands for the extension as shown in the figure 1(b). Table 1 summarizes the characteristics of precursor material and TCP muscles for use in our orthotic hand. We have studied this muscle extensively in one of our recent work [44]. For convenience throughout this paper, we will refer the muscle as twisted and coiled polymer (TCP) muscles. These TCP muscles display larger stroke and higher power to weight ratio than conventional actuators and have minimal hysteresis. Lower hysteresis makes the control for the TCP based systems easier and simpler. Few papers are emerging on the control of TCPs and showing the benefits of less hysteresis [49, 50]. SMAs are very difficult to control as described by other researchers [51, 52]. This is mainly due to the requirement of switching function to represent the phase transformation in the material that resulted high hysteresis loop in the stress strain curve.

2.3. Fabrication and characterization of artificial muscles

TCP muscles were prepared in a similar way as described in Saharan *et al* [44], and Wu *et al* [48]. Briefly, the TCP muscle fabrication consists of the following steps: (i) twist insertion in the commercial thread (here 800 rpm, at 175 g load was used); (ii) plying of the TCP into 2 ply; (iii) electrothermal annealing and training of the coiled fiber at 0.6 A of current (voltage varies based on length) for 50 s, at 400 g load, for 8 cycles with a 50% duty cycle. The ratio of original, non-twisted fiber length to coiled length for the investigated yarns is about 3.5. The plying is done by folding the muscle halfway and letting it untwist so that muscles gets plied due to the release of twist in the opposite direction. The performance of the muscle has been studied and described in some of our previous studies [44, 48, 53].

For further study on muscle behavior, we have investigated the thermal degradation of the precursor material, as well as the heating element thickness. As received Ag-plated nylon 6,6 multifilament thread was analyzed by scanning electron microscope (Zeiss–LEO Model 1530 scanning electron microscope) coupled with EDX to verify the thickness of the heating element coating. The sample was coated with gold by sputtering prior to analyses.

Thermal degradation study of the Ag-plated nylon 6,6 multifilament threads was carried out in TA Instruments Q600 and TA Instruments Q2000 for thermo gravimetric (TGA) and differential scanning calorimeter (DSC) analyses,

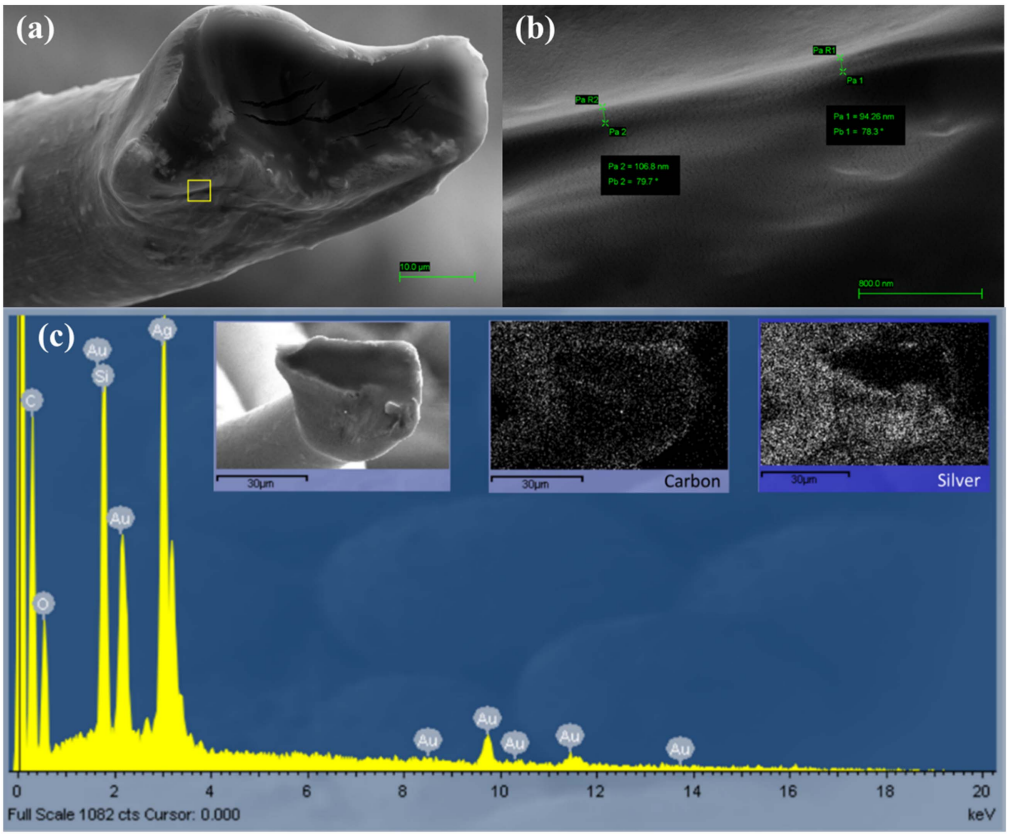

Figure 2. Micrograph of (a) unique filament from as received Ag-plated nylon 6,6 multifilament thread; (b) silver coating detail magnified from (a); and (c) Energy dispersive spectrum of as received Ag-plated nylon 6,6 with inserted SEM micrograph of cross-section of the filament analyzed and its mapping for carbon and silver elements.

respectively. For both TGA and DSC measurements, the samples (~8.7 mg and ~2.6 mg, respectively) were degraded under a nitrogen flow of 50 mL min^{-1} at heating/cooling rate of 10 °C min^{-1}.

2.4. Heating element analyses of Ag-plated nylon 6,6 multifilament

Scanning electron micrographs (figure 2) illustrate the asymmetrical cross-section of a filament from the as received Ag-plated nylon 6,6 multifilament thread. The observations (figure 2(b)) suggest the silver heating element for TCP muscle is around 100 nm in thickness.

Energy dispersive spectroscopy of as received Ag-plated nylon 6,6 (figure 2(c)) identified that the plated coating is pure silver. Silicon signal is due to silicon wafer used as a substrate.

2.5. Thermal analyses of Ag-plated nylon 6,6 multifilament

DSC thermogram of as received Ag-plated nylon 6,6 multifilament thread (figure 3(a)) show crystalline melting temperature (Tm) and crystallization temperature (Tc) of 254 °C and 227 °C, respectively. These temperatures are similar to that reported by Pramanik *et al* [54] once a cross-linker and e-beam irradiation are used in the preparation of nylon 6,6 to improve mechanical properties and reduce water absorption.

TGA thermogram of as received Ag-plated nylon 6,6 multifilament thread (figure 3(b)) shows that the temperature of its maximum rate of degradation (T_{max}) is around 449 °C. Pramanik *et al* also observed similar value once crosslinking of nylon 6,6 was increased by e-beam irradiation. The degradation starts around 375 °C and gets completed around 485 °C. Thus, Ag-plated nylon 6,6 in a nitrogen atmosphere is considered thermally stable up to 375 °C with almost complete decomposition at 485 °C. Komolan *et al* [55] observed a slightly lower range of thermal degradation for virgin nylon 6,6 (started at 368 °C and finalized at 470 °C). According to the literature [56, 57], the nylon 6,6 degradation is based on the cyclization of the adipic acid groupment in the polymer, resulting in cyclic products and carbon dioxide. Once in inert atmosphere, above the melting point of the polymer, water, carbon dioxide, and cyclopentanone are the main products.

3. Design and manufacturing of hand orthosis

3.1. Anatomically correct testbed hand

Before doing the human subject test and to have freedom of performing a full range of experiments, we made a dummy hand for experimentation. Inspired by the work of Deshpande *et al* [58], on anatomically correct test-bed hand, we decided to design an anatomically accurate skeleton hand, which can

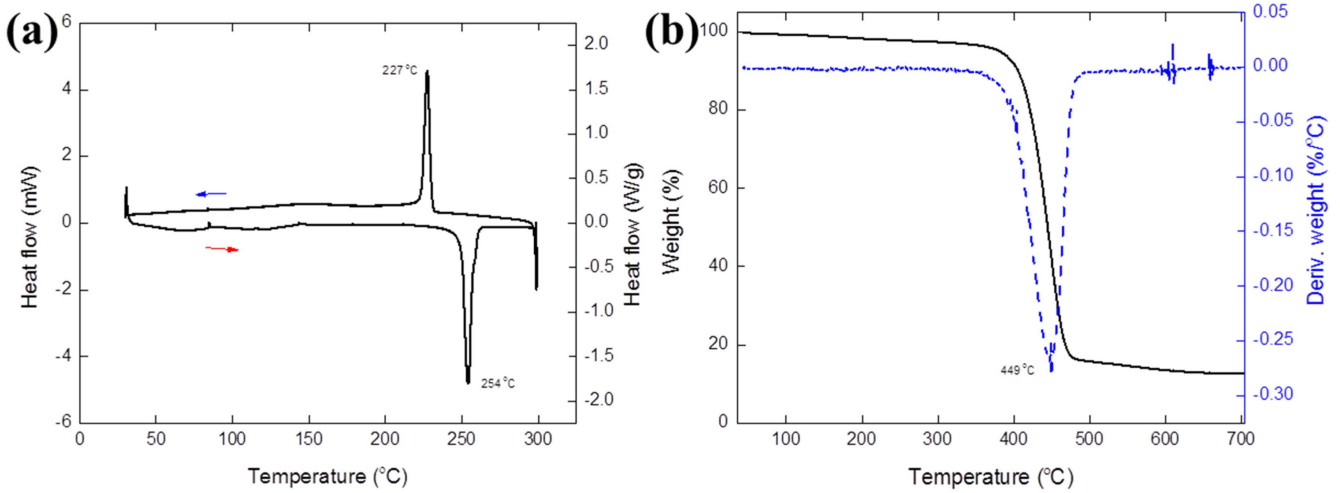

Figure 3. Thermo-mechanical properties of as received Ag-plated nylon 6,6 multifilament thread (a) DSC thermogram, (b) TGA thermogram.

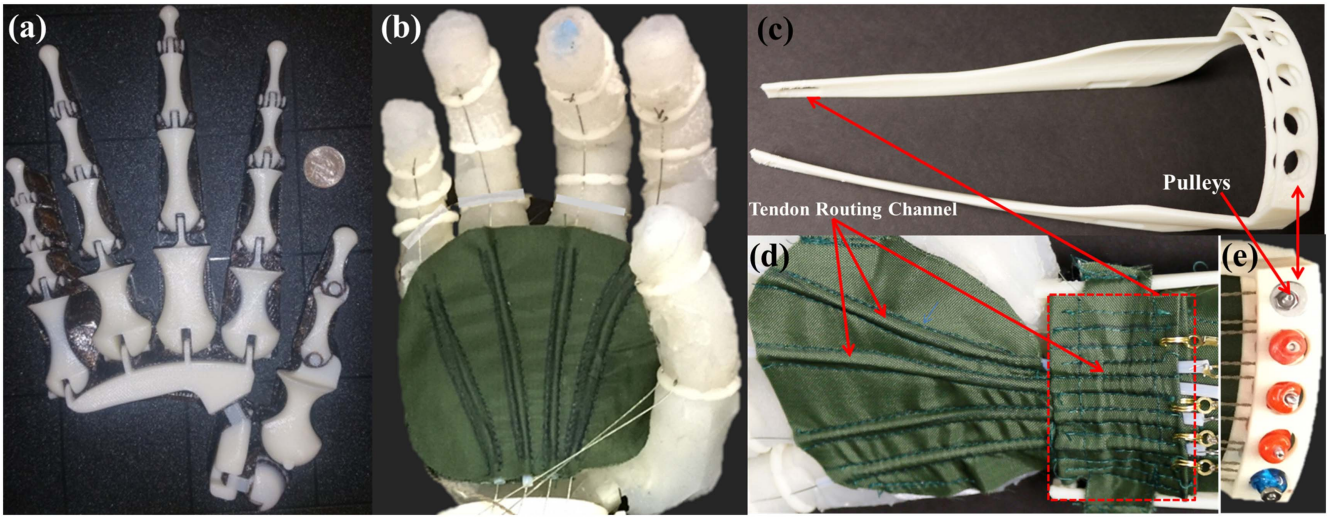

Figure 4. (a) 3D printed hand skeleton, (b) Hand after Silicone casting and assembly, (c) 3D printed base for the exoskeleton, (d) Tendon routing mechanism in palm and wrist where the cloth was sewed to create a channel for routing PTFE (Teflon) tube which allows smooth movement of tendons. (e) Pulleys placed in the hubs which allow wrapping of the muscles to facilitate longer lengths.

be 3D printed and embedded within silicone by casting to have the same configuration as a human hand. This anatomically correct hand was used throughout the study to perform various experiments at UT Dallas as well as Lynntech Inc.

The skeleton was made to have similar features as human hand skeleton including ball and socket for the thumb to mimic human thumb motion. This silicone cast hand was later mounted on a 3D printed arm similar to the human hand as shown in figure 4. The arm was also designed in Solidworks®, and 3D printed using Fortus 250 MC. The arm has dimensions similar to an average adult size hand.

3.2. Force and tendon displacement requirements

The force required for flexion and extension of a human finger was found from literature, and it was reported in references [59] and [60] that the amount of safe force required for the hand is from 1 to 3 N. Some patients might need more power in their orthosis. One way to measure the necessary force is to suspend a weight on a human subject's finger and track the angle versus load, and then determine the maximum amount that produces the maximum flexion. Another possible way is to take mean measurements from a population of a certain age of people with similar physical features and the amount of force required. Later on, adjustments can be made based on different individual needs. Therefore, to make the orthotic device useful, we need to provide the fingers the required force and displacement (a corresponding angle) to flex the fingers and do the intended task. The forces and the angles required are used as some of the parameters in our design of orthotic hand module. Tendon displacement was measured experimentally for full flexion of all the fingers which is 60 mm for index and middle fingers and 50 mm for

ring and pinky finger. This information will allow calculating the length of the muscle and power requirements for individual fingers.

3.3. Design of iGrab hand orthosis

The device is comprised of 3D printed and sewed parts as shown in figure 1(a). Tendons routed to the wrist through 3D printed rings through PTFE pipe channels. Flexion motion is facilitated using TCP muscles mounted on the forearm. The TCP muscles are wrapped around pulleys as shown in the figure 4(e), to utilized longer muscle length for large strokes. Extension motion is facilitated with the help of rubber strips as shown earlier in figure 1(b). Rubber bands provide less stiffness than TCP muscle, thus yielding an energy efficient method for extension motion.

The exoskeleton was designed in CAD software and fabricated in two steps. The first part includes the 3D printing of exoskeleton arm base (figure 4(c)) and the rings. Later, PTFE pipes were sewed in fabric to route tendons from fingertips to wrist where all the TCP actuators are located. First, PTFE pipes (internal diameter of 1.5 mm) were routed through the sewed cloth (figure 4(d)). The stitched fabric keeps the device soft and adjustable in form/shape according to the patient. Rings were directly mounted on the fingers. Each ring has several holes of 2 mm in diameter. The inner diameters of the rings are small. For example, the rings for the little finger are 12, 18 and 20 mm in diameter. For all the rings, the outer diameters (D_o) are based on the following equation $D_o = D_i + t$, where Di is the inner diameter of the ring. The thickness (t) of each ring is 2 mm. The dimensions of the rings were set based on average adult man hand size and based on the available space between each finger. Once all the dimensions were checked to ensure that the structure would be 3D printable, the prototype was developed to test the design.

During integration, the passive tendon was crimped at one end to prevent it from slipping through the top ring (DIP). Then, the tendon was passed through the rings on the PIP and MCP joints before entering to PTFE channels on the palm. The ring holes were already very smooth due to appropriate fillet provided in the design. The tendon is nowhere fixed on any ring except the first one, the two rings just acted as a guide for the tendon. Hence, the full force was transmitted to the ring on the DIP joint. We experimentally measured the tendon displacement and the force required for a finger to flex completely and show the results in figure 5. We can see that 50 mm of tendon displacement is required to completely flex the ring finger. A force of 2.70 N is required to displace the tendon by 50 mm for the ring finger (figure 5(b)). This force is almost equal to the force produced by the muscle when integrated in the device (2.84 N). So, the force lost due to friction is around 0.14 N which is around 5% of the total force. We neglected this small frictional force for further modeling and analysis. The force requirement for flexing all the fingers is almost the same but the tendon displacement varies between 50–70 mm for different fingers. Another important issue is the offset distance, the tendon is at the offset distance of 4.4 mm from the center of the finger. Hence, the total torque caused by the muscle though this transmission system is 11.88 N-mm. We don't know the exact magnitude of torque at the individual joint because the system is underactuated. This issue will be later addressed in the dynamics section.

Initially, the connector plate between each ring was 3D printed using acrylonitrile butadiene styrene (ABS Plus). These structures were assumed to act as springs and help in the return motion of the finger during actuation. The sizes of the spring structures were 6 mm wide and 1 mm thick. The parameters of the structures were varied, and the flexibility was checked. These structures were later removed due to limited flexibility and snapping during testing. Two additional designs were also studied, but we are not discussing those in this paper.

Thumb plays a vital role in grasping of objects. We paid particular attention to the thumb design in dummy hand as well as in the exoskeleton. In the dummy hand, the thumb is designed using a modified ball and socket joint to replicate human thumb motion.

The full 3D printed exoskeleton system is light in weight. The wearable part is approximately 100 grams in weight for all five fingers, excluding the battery which is less and convenient for practical usage as compared to many of the existing orthotic devices.

3.4. Wrist design concept

The exoskeleton is designed to be soft and flexible. Ergonomic design will impact the quality of life for the user significantly. Our conceptual design of the wrist part of the exoskeleton is to have six different layers as shown in figure 6. Lowest layer close to the skin (1st layer) should be soft and comfortable. It should also be able to facilitate breathing for the skin. The second layer would be a pack of glass wool sewed in the cloth. Next to insulation layer will be heat dissipating layer (3rd layer) made up of some fins or mechanism to control the release of heat outside the enclosure. The 4th layer will be the TCP muscle. The 5th layer will also be a glass wool pack to protect the flexible electronics and battery in the 6th layer from heat generated by TCP muscle.

3.5. Thermal management

TCP muscles actuate the iGrab device when heated with electrical power that causes the muscles to contract and subsequently to expand when the electric power is turned off. The device is tendon driven wherein the muscles are enclosed within a worn forearm bracelet and are connected to tendons that run parallel to the length of the finger. The tendons are not electrically powered and do not experience temperature rise during device operation. Additionally, every part of the iGrab device that comes in contact with the user experiences no temperature rise and remain safe to touch during the device operation.

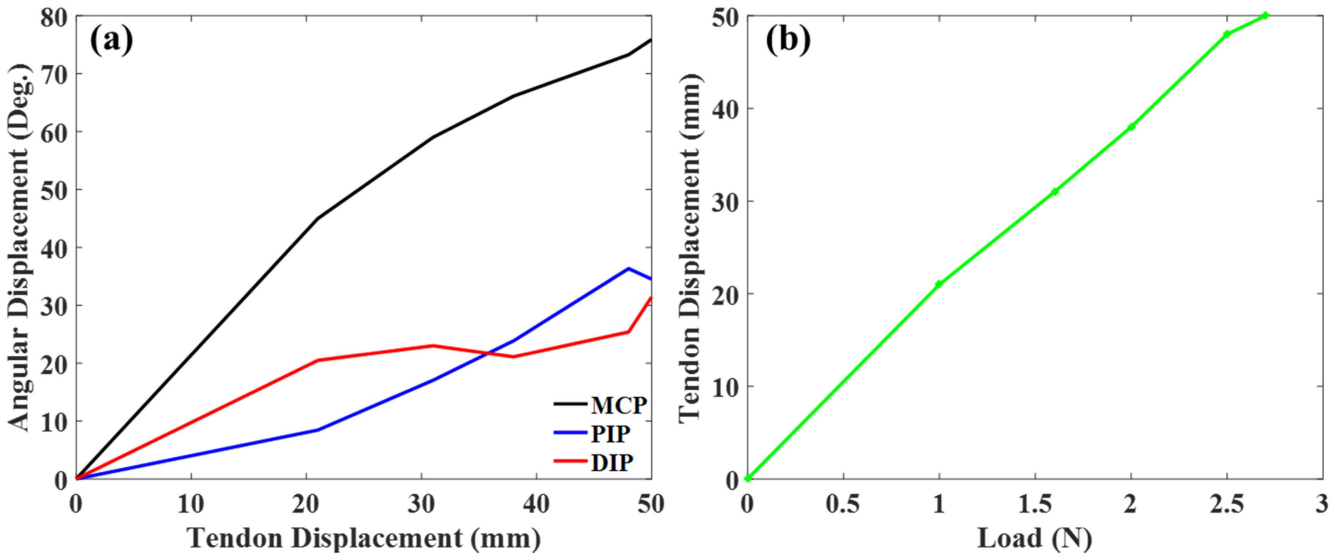

Figure 5. Angular displacement / tendon displacement / required force relationship of the dummy hand: (a) the tendon displacement and corresponding angle of each joint, and (b) the load required for the corresponding tendon displacement of a finger.

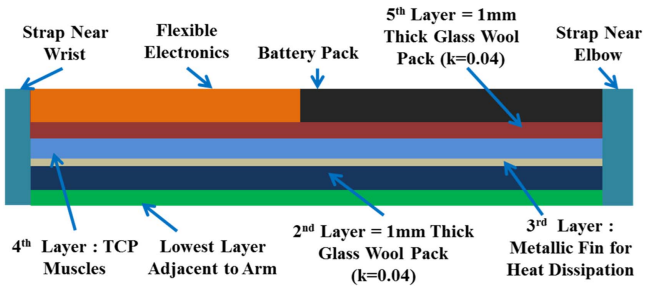

Figure 6. Shows the schematic of cross-sectional view of the envisaged glove wrist area.

TCP muscles have extremely low thermal mass (16 mg mm^{-1}), and this allows the muscles to cool down to ambient temperature within 2 s (at regular ambient condition). This cooling was both experimentally and analytically verified and was achieved just through exposure to ambient air conditions. Free convection heat transfer analysis was conducted assuming the simplified cylindrical geometry of artificial muscle (2-ply, 2 mm in diameter of 400 mm in length, schematically shown in figure 7(a)). The Nusselt number, Nu_D parameter for the thermal analysis is given by [61]:

$$Nu_D = \frac{\bar{h}D}{k} = \left\{0.60 + \frac{0.387(Ra_D)^{1/6}}{[1 + (0.559/Pr)^{9/16}]^{8/27}}\right\}^2 \quad (1)$$

Where $\bar{h}$ is convective heat transfer coefficient, k is the conductance, D is the diameter, Ra_D is Rayleigh number, Pr is the Prandtl number.

The heat transfer rate q_{conv} is given by:

$$q_{conv} = \bar{h}\, A\, \Delta T \quad (2)$$

Here A is the area and ΔT is the temperature change.

The time required to cool down the artificial muscle was determined using a relation as:

$$t_{cool} = \frac{P_{input\ to\ the\ muscle} \times actuation\ time}{q_{conv}} \quad (3)$$

Even though the muscles never come in contact with the skin, they will be safe to human touch. If desired, one can touch very quickly (<2 s) once the power is turned off. Additionally, the iGrab prototype design includes redundant safety features that further enhance the safety of the user.

3.6. Thermal insulation determination

To protect the human hand skin from the heat generated by the artificial muscles, the insulation material thickness was determined using heat transfer analysis based on experimental temperature data. It was determined that the instantaneous localized temperature on the artificial muscle could exceed 70 °C when given 10 W of total power. The temperature for pain threshold of human is 44 °C at the dermal/epidermal interface of the skin [62]; therefore, the required temperature at the interface of skin and the insulation was chosen as 40 °C. Assuming that the artificial muscles have simplified cylindrical geometry and emits heat through conduction (2-ply, 2 mm diameter of 400 mm length), the correlation for the thickness of the insulation and thermal conductivity of the material was determined to identify the best glove material with a required thickness to make the artificial muscles safe for human touch. The correlation was determined using Fourier's law for heat conduction through the layer of insulation given by:

$$t_{insu} = \frac{k_{insulation}(T_{max} - T_{threshold})A_{contact}}{q''} \quad (4)$$

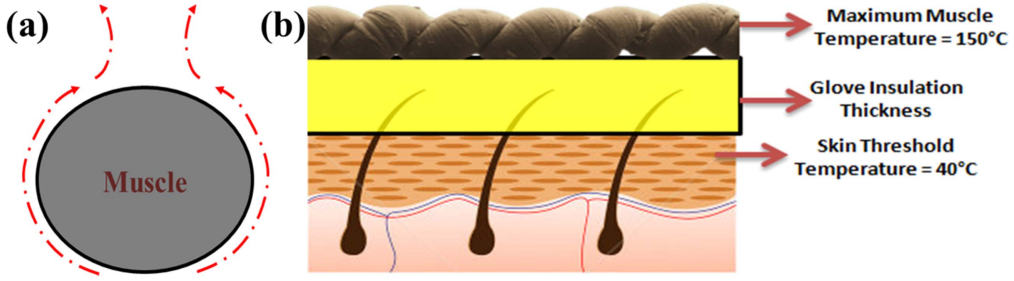

Figure 7. (a) Schematic diagram for free convection analysis of artificial muscles (b) Schematic for thermal insulation type and its thickness correlation.

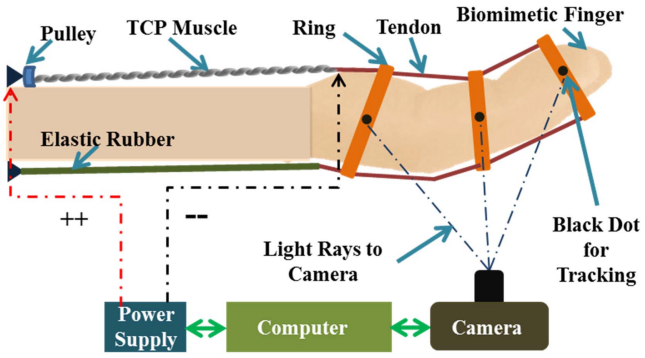

Figure 8. Schematic diagram of the experimental setup.

As described earlier, the threshold temperature was used as 40 °C whereas the maximum temperature was used as 150 °C. The heat flux was determined using the total surface area of the artificial muscle using cylindrical approximation with 2 mm diameter and 400 mm length of the muscle. The contact area then is assumed to be 50% of the total surface area from only one side of the muscle is exposed to the glove insulation at the skin interface as shown in figure 7(b).

3.7. Device portability

To determine the powering aspect of our device, we followed the work of Zheng *et al* [63], who recorded the motion of a fully capable house maid (29 type of Tasks) and a machinist (31 type of Tasks) for four hours. They used head-mounted camera for recording hand usage during daily work activities. We performed the calculation on the active activity time of the hand, number fingers involved in a particular task, instance (break periods) and classification of grasping provided in the paper. We determined the power required to restore the full functionality of these two types of workers using such a device like iGrab. We summed the total active time of fingers and found that 24 881 s for machinist and 27 712 s house maid are required. This suggests that all the fingers are not actuated for 4 h in daily activities (5 fingers actuated for 4 h would have required 72 000 s active time while using energy). If we consider the instances where the active time of the machinist and house maid, we find that the times are 5323 and 4677 s respectively. These times are used for the calculation of the device with locking mechanism. Results from the calculations are provided in table 2. The calculations were done assuming that regular actuation would require 15 V and 0.6 A for 25 s (225 J of energy) and a pulsed actuation requires 30 V and 1.5 A for 1 s (45 J of energy). For example, for house maid pulsed actuation without locking mechanism would require 27 712 s × 45 J, which is 1247 kJs (346 Wh), 30 V operating conditions requires 11 533 mAh of battery. For pulsed actuation with locking mechanism the energy is 4677 s × 45 J (58.46Whr), 30 V of operating conditions require 1948 mAh.

Therefore, we can clearly see that pulsed actuation with locking mechanism can restore the full working capability of a machinist or a house maid for approximately 6 h with addition of 650 grams of weight and $190 [64].

4. Experimental Setup

The experimental setup used to study the angular positions of the orthotic device includes an anatomically correct hand, high-speed camera (Phantom Miro), a computer with NI-cDaq data acquisition, a computer controlled power supply (BK Precision 1687b), and thermocouple (K-type) as shown in figure 8. The profile of the voltage waveform was programmed on a computer. The high-speed camera records the actuation motion of the orthotic hand, and later on, the data were extracted.

Experiments were performed using hand orthosis for all five digits by mounting them on the dummy hand and using step input voltage. The muscle parameters and input conditions are provided in table 3.

5. Results and discussion

Experimental results of the angular position of all joints of all the fingers: distal interphalangeal, proximal interphalangeal and metacarpophalangeal (DIP (θ_3), PIP (θ_2) and MCP (θ_1), respectively) for step input voltage are presented in figure 9. The results were obtained using the high-speed camera and PCC software that provide positions as well as speed data; the results are summarized in table 4. The angles provided in table 4 are absolute angles calculated to see the maximum values.

All the muscles were actuated at 0.6 A of current, and it was set not to exceed this current limit. MCP joint subtended almost the 40° for 25 s, whereas PIP and DIP could reach up

Table 2. Battery power requirements for orthotic device assuming 4 h daily activities.

Actuation Type	Power (mAh)		Battery Dimensions	Weight	Capacity (mAh)	Battery Price
	House Maid	Machinist				
Pulsed without LM	11 533	10 367	162 × 45 × 144 mm^3	2190 g	12 000	$620
Pulsed with LM	1948	2218	138 × 45 × 48 mm^3	639 g	3250	$190
Regular without LM	115 400	103 667	158 × 59 × 81 mm^3	1690 g	22 000	$499
Regular with LM	19 466	20 734	158 × 59 × 81 mm^3	1690 g	22 000	$499

*LM = Locking Mechanism ¥ LiPo Batteries for 4 h continuous working.

Table 3. Muscle parameters for test.

Parameter	Value
Input Voltage (V)	15
Input Current (A)	0.6
Time of actuation (sec)	25
Length of muscle (mm)	380
Resistance of the muscle (Ω)	9.7
Power supplied to the muscle V*A/L (W/m)	23.7

to 21° and 11° respectively for index finger (figure 9(a)). There was almost 6-degree motion in DIP joint for the middle finger but 31° for MCP joint and 25° for PIP joint (figure 9(b)). For ring finger, MCP and PIP have reached almost the steady state angle of 20° for 20 s. DIP has a slightly lesser angle of 12° (figure 9(c)). Similar to other fingers, Pinky has a small movement for DIP joint (11°). Angles for PIP and MCP joints are 14° and 40° respectively.

Figure 10 shows the angular displacement for the thumb where MCP joint has the largest angle of 35° in 6 s in the front view. The MCP joint for thumb also has motion in another plane that could not be captured by the camera. The PIP has the smallest angle of 12° whereas DIP moved 30°.

5.1. Effect of pulsed actuation in angular displacement of joints

Figure 11 shows the results of the measured angles in the second parametric study using pulsed actuation for all the fingers. In this experiment, the muscles are provided with an input pulse voltage for relatively short duration compared to the step input in the previous experiments. During the pulsed actuation, the rise time of angles decreases as we increase the pulse and maximum angle is also increased. All the pulsed actuation was done at 1.8 amperes of current for two seconds. As can be seen in the figure (figure 11), the maximum angles for each joint were achieved within 2 s.

5.2. iGrab repeatability of muscle force

Life cycle test was conducted on a muscle (length 400 mm and diameter 1.35 mm) by measuring the force generated while actuating a finger using a force sensor Omega LCL 010. The muscle was connected with the sensor, and the other end is attached to the tendon in the index finger. The results of the test are shown in figure 12. The test was conducted for 200 cycles continuously with each cycle 11 volt for 25 s (0.04 Hz) with 20% duty cycle. The force generated by the muscle was consistent over 200 cycles. The test was done over nearly 1.13 h. This result shows the uniform behavior of the muscle over the cycles. These results are very dense due to a full span of time, we showed voltage, current and force signal with magnification between 510th second and 550th seconds which consists of two cycles. For the given, voltage and current power can be seen consistently around 2 N.

5.3. Grasping experiments

Tests were conducted to check the grasping capability of the orthotic hand by actuating all the muscles in the iGrab and putting different objects in the palm while gravity is downwards. Figure 13 show this ability to hold, grasp and pinch objects firmly.

Some of these objects match the one provided in 'ABILHAND manual ability measure' [65]. For example, a screw headed jar (figure 13(b)), from the position in the picture, another hand can be used to twist and open the jar. The pant zipper can resemble precise handling of shuttle and chips packet can be torn open easily from the position in figure 13(g). We tried to squeeze toothpaste using the orthotic hand, but it slipped and flipped due to the very smooth surface. We also performed grasp, grip and pinching according to action research arm subscale as given in table A1 of [66].

6. Simulation and modeling

We have provided the dynamics of three links applied to robotic finger following the Euler–Lagrangian approach [53] along with a simulation of finger motions actuated by TCP muscles.

Figure 14 shows the free body diagram (FBD) of the finger with the orthotic device mounted on it, where tendons at offset distance, e enabling flexion of the finger due to muscle contraction. The Euler–Lagrangian modeling equations are as follows:

$$\frac{d}{dt}\frac{\partial L}{\partial \dot{q}_i} - \frac{\partial L}{\partial q_i} = \tau_i \tag{5}$$

Equation (5) is the standard Euler–Lagrange equation for robotic manipulators. It was adopted from [67]. The term 'L' is a difference of kinetic energy (K) and potential energy (P) as provided in equation (6).

$$L = K - P \tag{6}$$

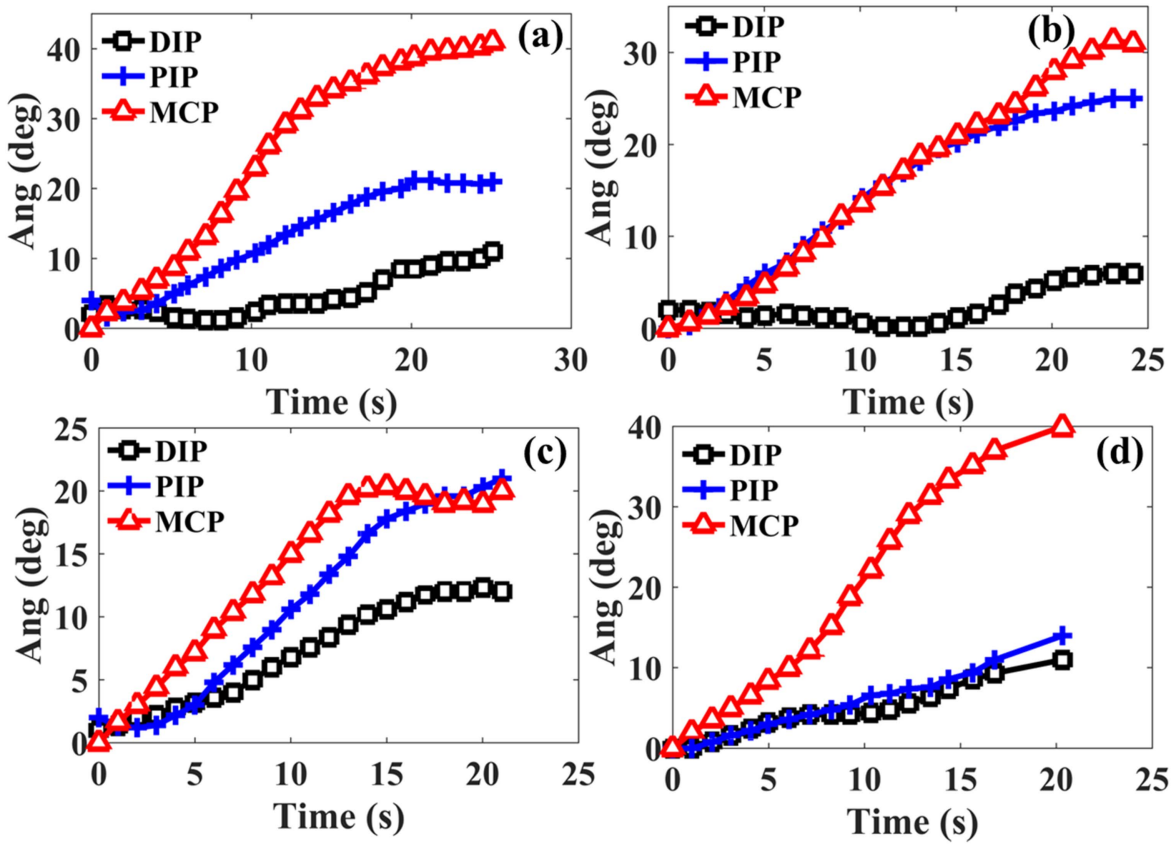

Figure 9. Angular displacement of the of the iGrab/dummy hand prototype measured using a fast camera Phantom® Miro for the test conditions in table 3 (a) index finger, (b) middle finger, (c) ring finger, and (d) pinky finger where three different joints are DIP (θ_3), PIP (θ_2) and MCP (θ_1). Muscles were triggered at 0.6 amps for 25 s at a duty cycle of 50%.

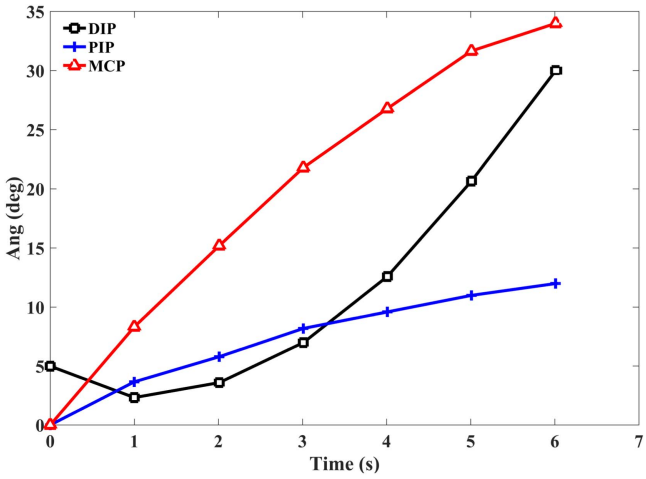

Figure 10. Angular position for thumb joints once the muscle is triggered according to table 2.

Table 4. Angular maximum displacement for each joint of all four fingers.

Joint	Motion	Index	Middle	Ring	Pinky
DIP	Flexion/Extension	11	6	12	11
PIP	Flexion/Extension	21	25	21	14
MCP	Flexion/Extension	41	31	20	40

$$K = \frac{1}{2} m_i v_i^T v_i + \frac{1}{2} w_i^T I w_i \tag{7}$$

This equation (7) can be written in the following form in case of a manipulator:

$$K = \frac{1}{2} \dot{q}^T D(q) \dot{q} \tag{8}$$

The potential energy (P) term is given by:

$$P = \sum_{i=1}^{n} P_i = \sum_{i=1}^{n} g^T r_{ci} m_i \tag{9}$$

Where: K = kinetic energy, P = potential energy, τ_i = input torque for the ith link, q_i = angular displacement the ith link (referred as θ_i in result plots), $\dot{q}_i$ = angular velocity of the ith link (referred as ω_i in result plots), r_{ci} = center of the mass of the ith link, q is the angular position vector $\mathrm{q} = [\mathrm{q}_1\, q_2\, q_3] = [\theta_1\, \theta_2\, \theta_3]$, $\dot{q}$ is the angular velocity vector $q = [\,\dot{q}_1\, \dot{q}_2\, \dot{q}_3] = [\,\dot{\theta}_1\, \dot{\theta}_2\, \dot{\theta}_3]$, m_i = mass of the ith link, and n = number of links.

The Euler–Lagrangian equation discussed above was solved using Simulink® 2016 using parameters provided in table 5.

The assumptions for modeling are taken form our previous work [53]: (1) Friction joints are smooth with negligible friction, (2) Passive tendons are moving smoothly through rings without jerks (3) Fingers have a uniform stiffness for all

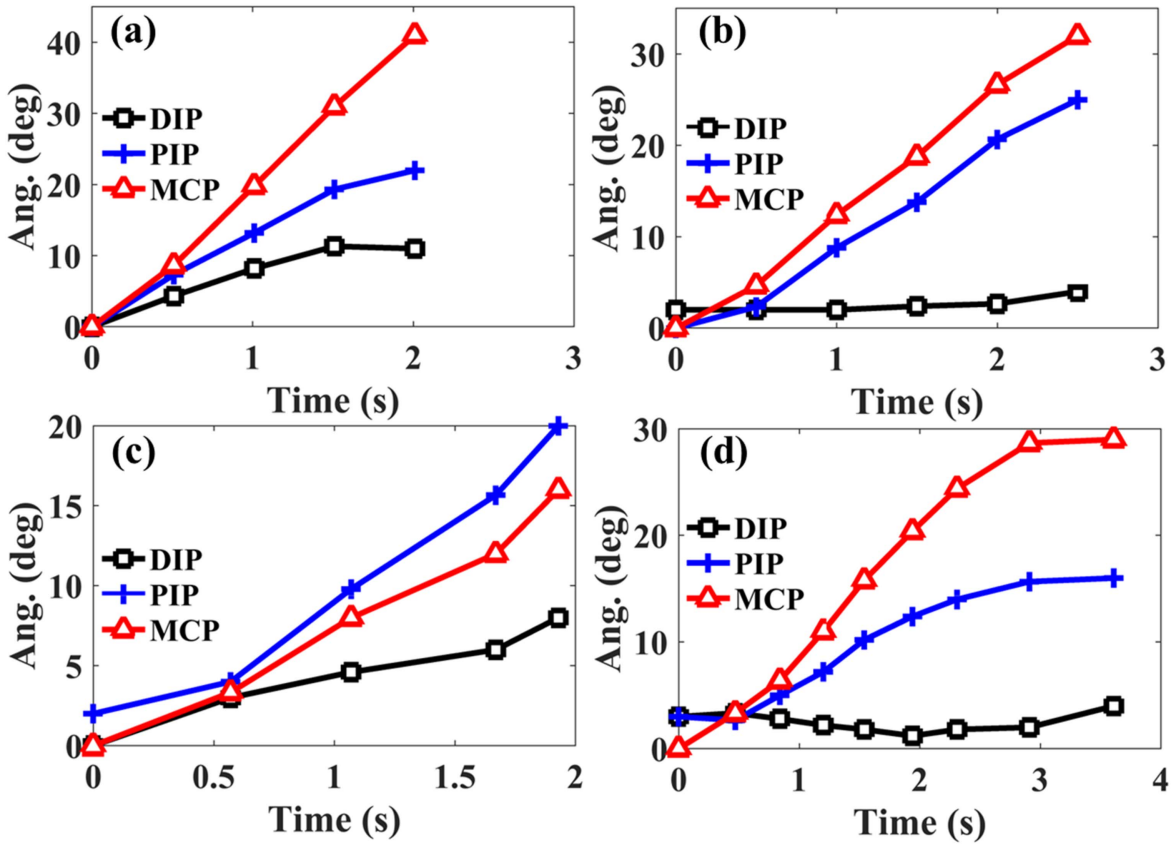

Figure 11. (a) Angular displacement of the iGrab/dummy hand for pulsed input power, the measured angles for DIP, PIP and MCP joints for two cycles. The muscles were triggered by 1.8 amps at a duty cycle of 7.4% for 27 s under natural cooling.

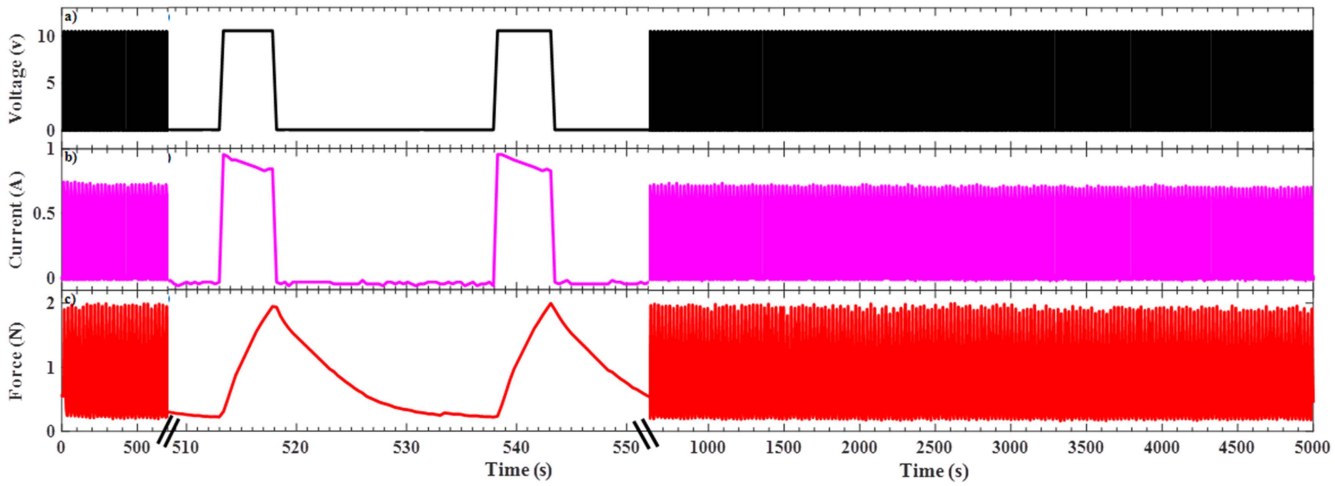

Figure 12. (a)–(c): Cyclic test for 200 cycles where 5 s power cycle and 20-second cooling cycle with a magnified view from 510 s to 550 s to show the profile of the data.

its joints, and (4) Input force profile is known previously using experimental measurements. Assuming the torque generated by the TCP actuator is distributed at each joint (τ_1 = MCP joint, τ_2 = PIP joint and τ_3 = DIP joint) with certain factors, the torques can be written as follows:

$$\tau_3 = \gamma.\tau;\ \ \tau_2 = \beta.\tau;\ \ \tau_1 = \alpha.\tau;\ \ \tau = F.e \qquad (10)$$

Where α, β, γ are a fraction of the torque experienced by each link, F is the force generated by the TCP muscle and e is the offset distance of the tendon. Though these fractions are not constant during the motion for the sake of simplicity we are assuming those to be constant having values equal to 0.73, 0.55 and 0.33. We have explained this equation in one of our recent work [53].

The simulations also consider damping factor with is an integral part of any mechanical systems. Several researchers have discussed damping in the human hand [68–70]. We have simulated the angular positions of the three joints of the ring

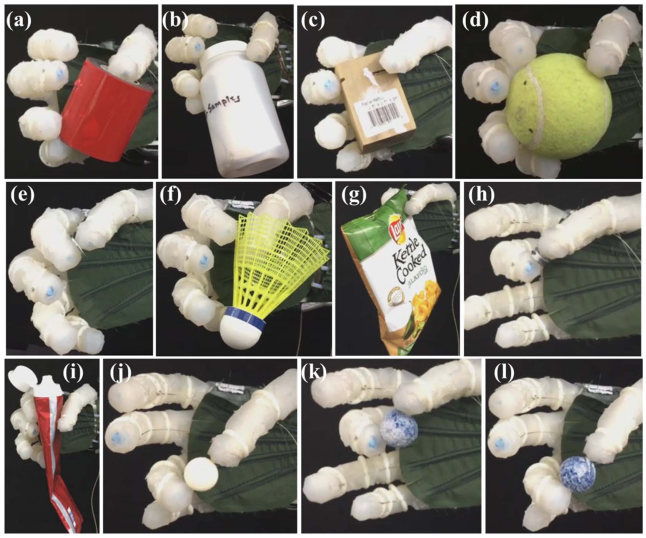

Figure 13. Grasping of daily used objects: (a) tape roll, (b) small plastic container, (c) wooden block, (d) tennis ball, (e) small rivet, (f) shuttlecock, (g) chips packet between ring finger and thumb, (h) small pulley, (i) toothpaste, (j) small disk between ring finger and thumb, (k) small ball between middle finger and thumb, and (l) small ball between ring finger and thumb. All the experiments are done against gravity, and hence gravity is acting downwards.

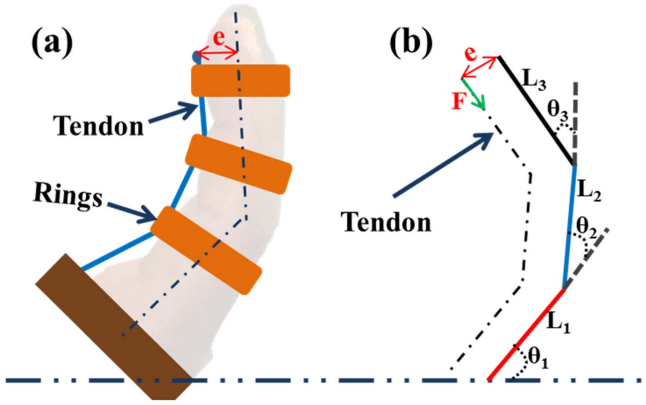

Figure 14. Dynamic model of the index finger: (a) Front view of the finger model with rings (b) Free body diagram, where 'e' is the offset from the central axis.

Table 5. Simulation parameters for the orthotic ring finger.

Parameter	Value	Parameter	Value
m_1	9.40×10^{-3} kg	LoL 1 (l_1)	0.036 m
m_2	6.67×10^{-3} kg	LoL 2 (l_2)	0.026 m
m_3	3.12×10^{-3} kg	LoL 3 (l_3)	0.019 m
MoI (I_1)	4.08×10^{-6} kg-m^2	Damping factor (c_d)	0.001
MoI (I_2)	2.27×10^{-6} kg-m^2	Input type	Experimentally Measured
MoI (I_3)	1.11×10^{-6} kg-m^2	Offset (e)	4.4×10^{-3} m
Simulation Time	50 s	Input Force (max)	2.84 N

*MoI = Moment of Inertia LoL = Length of Link M_i = Mass of Link.

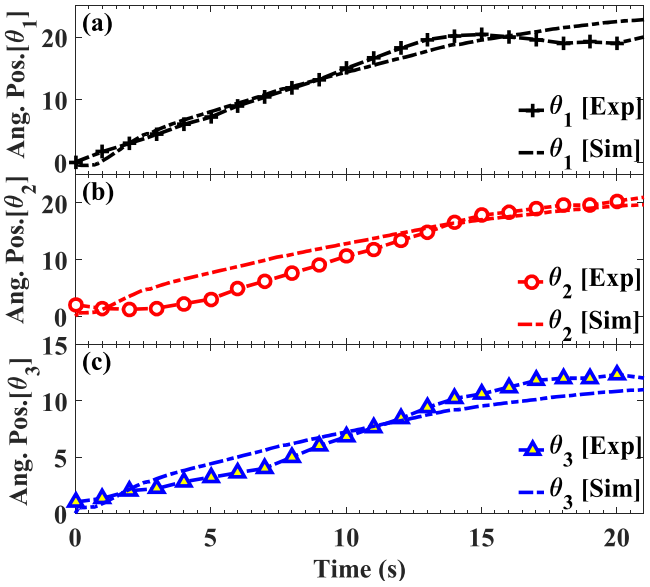

Figure 15. Comparison of the angular positions simulation with damping factor ($cd_1 = 0.001$) with the experimental results.

finger (figure 15) by considering damping factor ($C_d = 0.001$) to compensate different hand structures, mechanical design of orthotic device and usage. Results for angular displacement, experimental and simulated values, are seen to be relatively close to each other. The order of magnitude of the inertia, the mass and the length of the links in table 5 is small compared to the force and therefore one can ignore the angular acceleration.

7. Conclusion

In this paper, we demonstrated the design, characterization, modeling and validation of novel orthotic hand called iGrab. The orthotic device was mounted on a biomimetic hand and tested for grasping, holding and pinching capabilities of various objects with different shapes and sizes. The model was developed in CAD software and 3D printed, integrated with a technical textile (for thermal management purposes) containing sewed tendon channels. Our approach allowed to fabricate the lightest hand orthosis ever reported (100 grams without batteries) for all five fingers including multi-directional thumb control and for the first time, a TCP muscle powered orthosis. We demonstrated that iGrab is capable of mimicking the basic movements of a finger, including flexion and extension while keeping its force output over 200 cycles. Thermo-mechanical analysis of the muscle showed the crystallization of the precursor material (nylon 6,6) to be 227 °C, and melting temperature of 254 °C and starts decomposing on 375 °C. The precursor fiber for muscle fabrication has a 100 nm thickness of silver. The dynamic performance of the device was studied using Euler–Lagrangian modeling and simulation, which were matched with experimental results. A dynamic model would help in the control of the device. The next steps in this work include the inclusion of a locking mechanism to increase the power efficiency of the device and

design modifications to improve actuation and thermal management. Pulsed actuation with forced cooling would be the key to achieve high-frequency motion. Prospective users with muscle and nerve disorders could benefit from the iGrab device once it is fully developed.

Acknowledgments

The paper is submitted on 05/08/2017. This material is based upon work supported by the US Army Medical Research and Material Command under Contract no. W81XWH-15-C-0023. The views, opinions, and/or findings contained in this report are those of the authors and should not be construed as an official Department of the Army position, policy or decision unless so designated by other documentation.

References

[1] *Statistics on Hand and Arm Loss*. 1996 [cited 2015 10-3-15]; Available from: http://aboutonehandtyping.com/statistics.html
[2] Brook N *et al* 1995 A biomechanical model of index finger dynamics *Med. Eng. Phys.* **17** 54–63
[3] Sancho-Bru J *et al* 2001 A 3D dynamic model of human finger for studying free movements *J. Biomech.* **34** 1491–500
[4] Saggio G *et al* 2015 Resistive flex sensors: a survey *Smart Mater. Struct.* **25** 013001
[5] Aw K and McDaid A 2014 Bio-applications of ionic polymer metal composite transducers *Smart Mater. Struct.* **23** 074005
[6] Shahinpoor M and Kim K J 2001 Ionic polymer-metal composites: I. Fundamentals *Smart Mater. Struct.* **10** 819
[7] Lee S J *et al* 2006 A new fabrication method for IPMC actuators and application to artificial fingers *Smart Mater. Struct.* **15** 1217
[8] Fok K S and Chou S M 2010 Development of a finger biomechanical model and its considerations *J. Biomech.* **43** 701–13
[9] Battezzato A 2015 Kinetostatic analysis and design optimization of an n-finger underactuated hand exoskeleton *Mech. Mach. Theory* **88** 86–104
[10] Leijnse J and Spoor C 2012 Reverse engineering finger extensor apparatus morphology from measured coupled interphalangeal joint angle trajectories—a generic 2D kinematic model *J. Biomech.* **45** 569–78
[11] Amirabdollahian F *et al* 2014 Design, development and deployment of a hand/wrist exoskeleton for home-based rehabilitation after stroke-SCRIPT project *Robotica* **32** 1331–46
[12] Brokaw E B *et al* 2011 Hand spring operated movement enhancer (HandSOME): a portable, passive hand exoskeleton for stroke rehabilitation *Neural Systems and Rehabilitation Engineering, IEEE Transactions on* **19** 391–9
[13] Flores-Luna R I *et al* 2014 Semi active hand orthosis *ASME 2014 Int. Mechanical Engineering Congress and Exposition* (American Society of Mechanical Engineers)
[14] Cincotti C *et al* 2015 Strength amplifying hand exoskeleton *Biomedical Engineering Conf. (NEBEC), 2015 41st Annual Northeast* (IEEE)
[15] Hoffman H B and Blakey G L 2011 New design of dynamic orthoses for neurological conditions *NeuroRehabilitation* **28** 55
[16] Macovei S and Doroftei I 2016 A short overview of upper limb rehabilitation devices *IOP Conf. Series: Materials Science and Engineering* (IOP Publishing)
[17] Jones C L *et al* 2014 Design and development of the cable actuated finger exoskeleton for hand rehabilitation following stroke *Mechatronics, IEEE/ASME Transactions on* **19** 131–40
[18] Cempini M, Cortese M and Vitiello N 2015 A powered finger-thumb wearable hand exoskeleton with self-aligning joint axes *Mechatronics, IEEE/ASME Transactions on* **20** 705–16
[19] Baker M *et al* 2011 Orthotic hand-assistive exoskeleton *Bioengineering Conf. (NEBEC), 2011 IEEE 37th Annual Northeast* (IEEE)
[20] Baqapuri H I *et al* 2012 Prefabrication design of an actuated exoskeleton for traumatized and paralytic hands *Robotics and Artificial Intelligence (ICRAI), 2012 Int. Conf. on* (IEEE)
[21] Goutam S and Aw K C 2014 Development of a compliant hand assistive device *Mechatronic and Embedded Systems and Applications (MESA), 2014 IEEE/ASME 10th Int. Conf. on*
[22] Colon M *et al* 2014 3-D printed hand assisstive exoskeleton for actuated pinch and grasp *Northeast Bioengineering Conf. (NEBEC), 2014 40th Annual*
[23] Lee S, Landers K and Park H-S 2014 Development of a biomimetic hand exotendon device (BiomHED) for restoration of functional hand movement post-stroke *Neural Systems and Rehabilitation Engineering, IEEE Transactions on* **22** 886–98
[24] Zhou M and Ben-Tzvi P 2015 RML glove: an exoskeleton glove mechanism with haptics feedback *IEEE/ASME Trans. Mechatronics* **20** 641–52
[25] Weiss P *et al* 2014 Parametrization of an exoskeleton for robotic stroke rehabilitation *Replace, Repair, Restore, Relieve–Bridging Clinical and Engineering Solutions in Neurorehabilitation* (Cham: Springer) pp 833–43
[26] Surendra W, Tjahyono A and Aw K C 2012 Portable and wearable five-fingered hand assistive device *Mechatronics and Machine Vision in Practice (M2VIP), 2012 19th Int. Conf* (IEEE)
[27] Villa-Bedoya J and Petroff N 2007 Development of an electro-mechanically controlled hand orthosis for assisting finger extension in stroke survivors *Revista Ingeniería Biomédica* **1** 48–54
[28] Hyunki I *et al* 2015 Exo-glove: a wearable robot for the hand with a soft tendon routing system *Robotics Automation Magazine, IEEE* **22** 97–105
[29] Kudo S *et al* 2014 Electric-powered glove for CCI patients to extend their upper-extremity function *System Integration (SII), 2014 IEEE/SICE Int. Symp. on* (IEEE)
[30] Aubin P M *et al* 2013 A pediatric robotic thumb exoskeleton for at-home rehabilitation: the isolated orthosis for thumb actuation (IOTA) *Rehabilitation Robotics (ICORR), 2013 IEEE Int. Conf. on* (IEEE)
[31] Ochoa J M and Kamper D 2009 Development of an actuated cable orthotic glove to provide assistance of fi nger extension to stroke survivors *Revista Ingeniería Biomédica* **3** 75–82
[32] Bryant M F 2016 *Myoelectric hand orthosis* US Patent No. 9,387,112
[33] Tadesse Y, Hong D and Priya S 2011 Twelve degree of freedom baby humanoid head using shape memory alloy actuators *Journal of Mechanisms and Robotics* **3** 011008
[34] Tadesse Y *et al* 2012 Hydrogen-fuel-powered bell segments of biomimetic jellyfish *Smart Mater. Struct.* **21** 045013
[35] Haines C S *et al* 2014 Artificial muscles from fishing line and sewing thread *Science* **343** 868–72
[36] Sharafi S and Li G 2015 A multiscale approach for modeling actuation response of polymeric artificial muscles *Soft matter* **11** 3833–43
[37] Kianzad S *et al* 2015 Nylon coil actuator operating temperature range and stiffness *Proc. SPIE* **9430** 94301X

[38] Mirvakili S M *et al* 2014 Simple and strong: twisted silver painted nylon artificial muscle actuated by Joule heating *Proc. SPIE* **9056** 90560I
[39] Kianzad S *et al* 2015 Variable stiffness structure using nylon actuators arranged in a pennate muscle configuration *Proc. SPIE* **9430** 94301Z
[40] Cherubini A *et al* 2015 Experimental characterization of thermally-activated artificial muscles based on coiled nylon fishing lines *AIP Adv.* **5** 067158
[41] Yang Q and Li G 2016 A top-down multi-scale modeling for actuation response of polymeric artificial muscles *J. Mech. Phys. Solids* **92** 237–59
[42] Wu L *et al* 2015 Nylon-muscle-actuated robotic finger *Proc. SPIE* **9431** 94310I
[43] Wu L *et al* 2016 A deformable robot with tensegrity structure using nylon artificial muscle *Proc. SPIE* **9799** 97993K
[44] Saharan L and Tadesse Y 2016 Fabrication parameters and performance relationship of twisted and coiled polymer muscles *ASME 2016 Int. Mechanical Engineering Congress and Exposition* (American Society of Mechanical Engineers)
[45] Tomar A and Tadesse Y 2016 Multi-layer robot skin with embedded sensors and muscles *Proc. SPIE* **9798** 979809
[46] Saharan L and Tadesse Y 2016 Robotic hand with locking mechanism using TCP muscles for applications in prosthetic hand and humanoids *Proc. SPIE* **9797** 97970V
[47] Saharan L *et al* 2017 Design of a 3D printed lightweight orthotic device based on twisted and coiled polymer muscle: iGrab hand orthosis *Proc SPIE* **10164** 1016428
[48] Wu L *et al* 2017 Compact and low-cost humanoid hand powered by nylon artificial muscles *Bioinsp. Biomim.* **12** 026004
[49] Takagi K *et al* 2017 Position control of twisted and coiled polymer actuator using a controlled fan for cooling *Proc. SPIE* **10163** 101632V
[50] Yip M C and Niemeyer G 2017 On the control and properties of supercoiled polymer artificial muscles *IEEE Transactions on Robotics* **33** 689–99
[51] Moallem M and Tabrizi V 2009 Tracking control of an antagonistic shape memory alloy actuator pair *IEEE Trans. Control Syst. Technol.* **17** 184–90
[52] Nakatani M *et al* 2003 3D form display with shape memory alloy *Proc. 13th Int Conf on Artificial Reality and Telexistence*
[53] Saharan L, Wu L and Tadesse Y 2017 Modeling and simulation of compact and low-cost humanoid hand powered by nylon artificial muscles—Euler-Lagrangian approach *IEEE Transactions on Mechatronics* Submitted
[54] Pramanik N *et al* 2011 Modification of nylon 66 by electron beam irradiation for improved properties and superior performances *J. Appl. Polym. Sci.* **122** 193–202
[55] Komalan C *et al* 2008 Thermogravimetric and wide angle X-ray diffraction analysis of thermoplastic elastomers from nylon copolymer and EPDM rubber *Polym. Degrad. Stab.* **93** 2104–12
[56] Wiloth F 1971 For thermal decomposition of nylon 6.6. Measurements for thermolysis of nylon 6.6 and 6.10 *Die Makromolekulare Chemie* **144** 283–307
[57] Wiloth F and S E 1970 Thermal degradation of nylon 66. 2. thermolysis of n-normal-hexyl-2-normal-hexylimino) cyclopentane-1-carboxamide-elimination of isocyanate from alpha-carbamoylcyclopentanimines *Chemische Berichte-Recueil* **103** 757
[58] Deshpande A D *et al* 2013 Mechanisms of the anatomically correct testbed hand *Mechatronics, IEEE/ASME Transactions on* **18** 238–50
[59] Cooper C 2013 *Fundamentals of Hand Therapy: Clinical Reasoning and Treatment Guidelines for Common Diagnoses of the Upper Extremity* (St Louis, MO: Elsevier)
[60] Tjahyono A P *et al* 2013 A five-fingered hand exoskeleton driven by pneumatic artificial muscles with novel polypyrrole sensors *Industrial Robot: An International Journal* **40** 251–60
[61] Jiji M L 1998 *Heat Transfer Essentials* (New York: Bengall)
[62] Greene L, Alden J and Hardy J 1958 Adaptation to pain *Federation Proc.* Federation Amer Soc Exp Biol 9650 Rockville Pike, Bethesda, MD 20814-3998
[63] Zheng J Z, Rosa S D L and Dollar A M 2011 An investigation of grasp type and frequency in daily household and machine shop tasks *Robotics and Automation (ICRA), 2011 IEEE Int. Conf. on* (IEEE)
[64] *8S LiPo battery* 29.6v www.maxamps.com
[65] Penta M, Thonnard J-L and Tesio L 1998 ABILHAND: a Rasch-built measure of manual ability *Archives of physical medicine and rehabilitation* **79** 1038–42
[66] Yozbatiran N, Der-Yeghiaian L and Cramer S C 2008 A standardized approach to performing the action research arm test *Neurorehabilitation and neural repair* **22** 78–90
[67] Spong M W, Hutchinson S and Vidyasagar M 2006 *Robot modeling and control* (New York: Wiley)
[68] Hajian A Z and Howe R D 1997 Identification of the mechanical impedance at the human finger tip *Journal of biomechanical engineering* **119** 109–14
[69] Morita T and Sugano S 1995 Design and development of a new robot joint using a mechanical impedance adjuster *Robotics and Automation, 1995. Proc., 1995 IEEE Int. Conf. on* (IEEE)
[70] Sugano S and Tsuto S 1992 Force control of the robot finger joint equipped with mechanical compliance adjuster *Intelligent Robots and Systems, 1992., Proc. of the 1992 lEEE/RSJ Int. Conf. on* (IEEE)